Oceanologia (2015) 57, 293—307

Available online at www.sciencedirect.com

ScienceDirect

journal homepage: www.elsevier.com/locate/oceano

ORIGINAL RESEARCH ARTICLE

Sea-level change and projected future flooding along the Egyptian Mediterranean coast

Mohamed Shaltout [a,c,*], **Kareem Tonbol** [b], **Anders Omstedt** [c]

[a] *Department of Oceanography, University of Alexandria, Alexandria, Egypt*
[b] *Meteorology Program, College of Maritime Transport and Technology, Arab Academy for Science, Technology and Maritime Transport, Alexandria, Egypt*
[c] *Department of Marine Sciences, University of Gothenburg, Gothenburg, Sweden*

Received 9 March 2015; accepted 23 June 2015
Available online 17 July 2015

KEYWORDS
Sea level;
Egyptian Mediterranean coast;
Nile Delta;
Climate change

Summary Future sea-level changes along the Mediterranean Egyptian coast (southern Levantine sub-basin) are projected using satellite altimetry data and model simulations. Twenty-one years (1993—2013) of satellite altimetry data, represented by dynamic topography (DT), are examined in light of tide-gauge observations. Current DT changes are examined with respect to five atmospheric/oceanic factors. The qualities of three realizations of the Geophysical Fluid Dynamics Laboratory (GFDL) model are examined by comparing these with DT. Finally, the simulations best describing the present DT are used to describe projected sea-level changes in the study area.

The results indicate that DT can be used to study coastal and deep-water sea-level changes in the study area. The southern Levantine sub-basin sea level has recently risen by an average of 3.1 cm decade^{-1} and exhibits significant annual sea-level variation of −17 cm to 8 cm. The sea-level variation is significantly affected by several factors: sea-level variation west of the Gibraltar Strait, steric sea level, and sea-surface temperature. The GFDL simulations best describing the recent sea level over the study area, i.e., GFDL-CM3 and GFDL-ESM2M, are used to calculate the two-model ensemble mean (GFDL-2ENM), which indicates that Egypt's Mediterranean coast will experience substantial sea-level rise (SLR) this century. The estimated uncertainty over the study area was 4—22 cm by 2100, with the emission assumptions dominating the three sources of

* Corresponding author at: Faculty of Science, Department of Oceanography, University of Alexandria, Alexandria, Egypt. Tel.: +20 1121501764.
E-mail address: Mohamed.shaltot@alexu.edu.eg (M. Shaltout).
Peer review under the responsibility of Institute of Oceanology of the Polish Academy of Sciences.

Production and hosting by Elsevier

http://dx.doi.org/10.1016/j.oceano.2015.06.004

uncertainty sources. Comparing the projected SLRs with digital elevation data indicates that Egypt's Mediterranean coast will only be safe from flooding by 2100 if effective adaptation methods are applied.

1. Introduction

The Egyptian coast is connected to the Mediterranean through the southern Levantine sub-basin, which extends from 25°E in the west to 34.5°E in the east (Fig. 1). The Egyptian Mediterranean coastal area includes five large lakes as well as tourist resorts, historical sites, fertile agricultural lands, and economic resources such as natural gas. This coastal zone is considered one of the five regions expected to experience the worst effects of a sea-level rise (SLR) of 1.0 m (Dasgupta et al., 2009). El-Raey (2010) estimated that even with an SLR of only 0.5 m, nearly all the Nile Delta beaches and approximately 30% of the cities of Alexandria and Port Said will be eroded and damaged.

The southern Levantine sub-basin and particularly the Nile Delta coast are of special economic and social importance. This is mainly because of these areas' high population densities, high poverty levels, and diversified economic activities, which include natural gas production, fishing, electricity generation, tourism, and agriculture. At the same time, this area is projected to experience harm from SLR, especially in the Nile Delta region, and an SLR of 0.5 m in the absence of effective adaptation could displace about two million people (El-Raey, 1997). According to the Egyptian Environmental Affairs Agency (1999) and Abu Hatab et al. (2012), the agricultural sector provides work for approximately 35% of Egyptians and produces 14.8% of Egyptian gross domestic product (GDP), the sector being especially important in the Nile Delta region. SLR will lower Egyptian GDP by harming the agricultural sector (Dasgupta et al., 2009) and changing the ecology of the coastal lake system (Palmer, 2008). Given the socioeconomic impact of rising sea levels, new and accurate international sea-level datasets have been launched over the past decade (e.g., using satellite dynamic height data) and several authors have studied dynamic sea-level change using these new datasets.

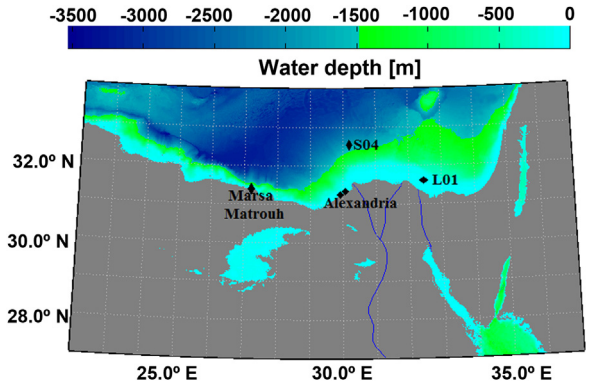

Figure 1 Bathymetric chart and observation sites (two stations near Alexandria).

The use of satellite altimetry data, represented by dynamic topography (DT), as a realistic tool for studying sea-level dynamics has been confirmed for open sea conditions only (Ducet et al., 2000; Volkov et al., 2007). The coastal altimetry signal is useful although it is less accurate than the open water altimetry signal (Rio et al., 2014). The accuracy of using DT data to capture coastal sea-level variation therefore still merits greater attention.

The Mediterranean sea level (MSL) has changed in recent decades, decreasing from 1960 to 1990 (Gomis et al., 2008) and then increasing from 1993 to 1999 (Cazenave et al., 2001). Cazenave et al. (2001) demonstrated that, except in the northern Ionian sub-basin, the sea level increased throughout the Mediterranean Sea between 1993 and 1999, and the authors expect this trend to increase in the future. Criado-Aldeanueva et al. (2008) found that the MSL changed, but insignificantly, over the 1999–2005 period. More recently, Tsimplis et al. (2013) found that the MSL rose significantly from 1993 to 2011 by approximately 3.0 cm decade^{-1}. Finally, Shaltout and Omstedt (2014) supported Tsimplis et al. (2013), finding that throughout the 1993–2010 period, the MSL displayed a significant positive trend of 2.6 cm decade^{-1}.

The MSL dynamics of the last two decades have been studied using satellite altimetry data. Cazenave et al. (2001) found that the MSL is significantly influenced by sea-surface temperature (SST). On the other hand, Quinn and Ponte (2010) demonstrated that sea-level changes are influenced by ocean mass changes and steric sea-level changes due to changes in water density (from changing salinity and temperature). In addition, Tsimplis et al. (2013) and Landerer and Volkov (2013) demonstrated that the MSL trend is influenced by several factors, such as ocean mass trends, North Atlantic Oscillation Index (NAOI) variations, and the wind setup (i.e., barotropic response) through the Gibraltar Strait. Shaltout and Omstedt (2014) found that the MSL is significantly affected by the sea level west of the Gibraltar Strait and by steric effects. However, the analyses of these earlier results in a limited domain, i.e., the southern Levantine sub-basin and along the Egyptian coast, merit additional research attention.

Some earlier studies of the southern Levantine sub-basin used tide-gauge data. At Alexandria, the annual mean sea level displayed a positive trend of 2 cm decade^{-1} from 1944 to 1989 (Frihy, 1992), 1.6 cm decade^{-1} from 1944 to 2001 (Frihy, 2003), and 3 cm decade^{-1} from 1974 to 2006 (Said et al., 2012). Alexandria's sea-level variation will be further discussed in Section 3.3.4. At Port Said, the annual mean sea level displayed a positive trend of 2.2 cm decade^{-1} from 1926 to 1973 (El-Fishawi and Fanos, 1989),

2.4 cm decade^{-1} from 1926 to 1987 (Frihy, 1992), and 2.3 cm decade^{-1} from 1926 to 1999 (Frihy, 2003). The trends clearly depend on the time interval studied, but an SLR is generally observed starting almost 90 years ago, before we expect to observe anthropogenic climate change due to increased greenhouse gas levels. Several factors may therefore need to be considered when attributing these trends.

Future scenarios for MSL dynamics have also been studied, and the Intergovernmental Panel on Climate Change's (IPCC's) first to fifth assessment reports discussed several possible future projections. The Coupled Model Intercomparison Project, phase-three (CMIP3) scenarios B1, A1B, and A2 are characterized by carbon dioxide equivalent concentrations in year 2100 of 600, 800, and 1,250 ppm, respectively. In the most recent IPCC studies, the Coupled Model Intercomparison Project, phase five (CMIP5) introduced scenarios RCP26, RPC45, RPC60, and RCP85, RCP standing for representative concentration pathway and the numbers indicating ten times the assumed radiative forcing at the end of the twenty-first century. According to Roaf et al. (2005), the global sea level is expected to rise by 30.0—80.0 cm over the 1990—2100 period. Meehl et al. (2007) illustrated the uncertainty of projected global SLR, which depends on the scenario used, projecting the global SLR during the twenty-first century to range from +28 cm decade^{-1} in the B1 scenario to +35 cm decade^{-1} in the A1B scenario. Tsimplis et al. (2008) demonstrated that the expected SLR of the Mediterranean Sea during the twenty-first century is 35 cm in scenario A2. The recent IPCC (2013, p. 90) assessment projects global sea-level changes as of the late twenty-first century based on 21 CMIP5 models, arriving at a mean increase of 40—63 cm and a range of 26—82 cm for emissions ranging from RCP26 to RCP85. Kopp et al. (2014) projected a global SLR of 30—120 cm between 2000 and 2100 for different CMIP5 RCP scenarios. Taylor et al. (2012) stated that the CMIP5 scenarios are expected to be improved compared with earlier CMIP runs; accordingly, we only use CMIP5 scenarios in the present study.

Most previous studies of the effect of SLR on the Nile Delta region examine only the assumed SLR range (El-Nahry and Doluschitz, 2010; Frihy, 2003; Hassaan and Abdrabo, 2013). The potential threats and impacts of SLR on the southern Levantine sub-basin, including the Nile Delta coast, therefore deserve greater attention. Moreover, local and global SLR can differ significantly (Kopp et al., 2014; Milne et al., 2009; Stammer et al., 2013), so regional assessments are needed for risk management, adaptation planning, and integrated coastal zone management (e.g., BACC II Author Team, 2015). Consequently, the current paper analyses the projected sea level over the southern Levantine sub-basin using dynamic calculations of the relevant global climate models (GCMs). Questions such as whether or not the Nile Delta will be flooded by the end of the twenty-first century merit considerable attention and will be discussed here.

The present analysis uses data from a 21-year period (1993—2013) for which gridded Mediterranean altimetry sea-level (i.e., DT) data are available. The study aims: (1) to examine the quality of the DT database used to study sea-level dynamics in the coastal area of the southern Levantine sub-basin; (2) to analyse temporal and spatial DT variability over the southern Levantine sub-basin; (3) to analyse the relationship between the study area DT data and other atmospheric and oceanic factors, such as barotropic response through the Gibraltar Strait, SST, sea-level variations west of the Gibraltar Strait, steric sea-level changes due to changes in water density, and changes in ocean mass; and (4) to examine the projected sea-level change in the study area up to 2100 using the available CMIP5 simulations of the GFDL model. The paper is structured as follows: Section 2 presents the material and methods used, Section 3 presents the results, and Section 4 discusses the results.

2. Material and methods

2.1. Data used

This paper discusses possible future changes in sea level in the coastal area of the southern Levantine sub-basin and along the Egyptian coast. The data used here include:

A) Satellite altimetry data and, in particular, gridded altimetry dynamic topography (DT) data: as DT represents the sum of sea-level anomalies plus the mean, it captures the geodetically corrected sea level (Rio et al., 2014). We used daily gridded DT data for the southern Levantine sub-basin (31—33°N and 21—35.5°E) with a 1/8° latitude/longitude spatial grid for the 1993—2013 period. The gridded DT data are merged from available multi-satellite altimetry data distributed by Archiving, Validation and Interpretation of Satellite Oceanographic data (AVISO; http://www.aviso.oceanobs.com/en/data.html). To study sea-level variability, the data are corrected for atmospheric pressure and wind effects (Ducet et al., 2000; Volkov et al., 2007).

B) Hourly sea levels observed at five stations (three along the Egyptian Mediterranean coast, one in the shallow-water zone, and one in the deep-water zone; Fig. 1) are used in examining the representative DT in the coastal area. Hourly sea-level observations from stations S04 and L01 (equipped with Aanderaa automatic meteorological stations) were obtained from Furgo GEOS for the periods May 1999—April 2000 and February 1999—January 2000, respectively. Time series of hourly tide-gauge data offshore of Alexandria, Egypt (31.22°N and 29.92°E) for 2010—2013 were extracted from the University of Hawaii Sea Level Center website (http://uhslc.soest.hawaii.edu/data/rqh). Hourly sea-level data for Alexandria Harbour (31.22°N and 30.1°E) from 1993 to 2005 and for Marsa Matrouh (31.37°N and 27.2°E) from 2004 were collected using mechanical tide gauges incorporating floats and counterweights.

C) Sea-level air-pressure data with a time resolution of 6 h acquired at the tide-gauge stations were extracted with a 0.75° × 0.75° spatial grid resolution from the ERA-Interim full-resolution dataset (http://apps.ecmwf.int/datasets/). Sea-level pressure (SLP) data are used to correct the tide-gauge data for the SLP effect.

D) Five atmospheric/oceanic processes were examined to determine their relationship with DT variability:
   1) The barotropic response through the Gibraltar Strait was calculated using ERA-Interim full-resolution (i.e., 0.75° × 0.75°) wind components through the Strait (http://apps.ecmwf.int/datasets/).

2) Sea-level variations west of the Gibraltar Strait over the Active Atlantic Mediterranean (AAM) sub-basin (33–37°N and 6–9°E) were extracted from the Aviso DT database with a 1/4° latitude/longitude spatial grid.
3) SST data were extracted from gridded daily AVHRR data (version 2) with a spatial grid resolution of 0.25° × 0.25° (http://www.ncdc.noaa.gov/oisst/data-access).
4) Daily vertical sea temperature and salinity data were extracted from the Mediterranean Sea Physical Analysis and Forecast database (Med-currents; http://marine.copernicus.eu/) covering the 1999–2013 period. The physical component of Med-currents is a coupled hydrodynamic-wave model implemented over the whole Mediterranean Basin. The model has a spatial grid resolution of 1/16° and 72 vertical levels (Oddo et al., 2009). Med-currents' physical properties agree well with semi-independent data (i.e., ARGO, CTD, XBT, glider, and Satellite SLA & SST data), according to Oddo et al. (2009). The Med-currents data are quasi-realistic and provide a reasonable tool for studying the physical properties of the Mediterranean Sea.
5) Ocean mass changes were extracted from the Gravity Recovery and Climate Experiment (GRACE) database of the Jet Propulsion Laboratory. The current GRACE gravity field coefficients (RL05) provide information about the amount of SLR caused by melting ice and changes in rainfall that add freshwater to the oceans. According to Chambers and Bonin (2012), the RL05 gravity coefficients are intended to improve the utility of the earlier gravity coefficients in ocean studies. Generally, a glacial isostatic adjustment (GIA) correction, a destriping filter, and a 300-km Gaussian filter are applied to the data. In addition, the leakage of land signals into the ocean is minimized by means of an iterative procedure (Landerer and Volkov, 2013; Tsimplis et al., 2013). According to Tsimplis et al. (2013), atmospheric pressure variations have an insignificant effect on the ocean mass redistributions, so GRACE data can be directly compared with DT values.

E) The climate model calculation of sea surface height above the geoid ("ZOS") for the 1860–2100 period was extracted from three model realizations: GFDL-CM3 (Griffies et al., 2011), GFDL-ESM2G (Dunne et al., 2012, 2013), and GFDL-ESM2M (Dunne et al., 2012, 2013). These model datasets are freely available via the GFDL database (http://nomads.gfdl.noaa.gov:8080/DataPortal/cmip5.jsp) for four CMIP5 emission scenarios. Inverse barometer corrections are not applied to the ZOS values, so barometric corrections are needed (Suzuki and Ishii, 2011). Moreover, monthly average simulated SLP results were extracted from the same realization used for ZOS in order to apply inverted barometer correction to ZOS. GFDL ZOS and GFDL SLP data have spatial grid resolutions of 1° × 1° and 2° × 2°, respectively.
F) Digital elevation data for the coastal area were extracted from the NASA Shuttle Radar Topographic Mission (SRTM) dataset with a 3-arc-second latitude/longitude spatial grid (version 4) (http://srtm.csi.cgiar.org). SRTM digital elevation data are used to discuss the flooding probability in the study area.

2.2. Methodology

2.2.1. Estimated quality of the DT database used in the coastal area

Rather than observed sea levels, direct correlations between the daily and monthly data on observed sea levels and gridded altimetry dynamic topography (DT) data are used to test the quality of the DT data used. The correlation coefficients (R) and number of observations (n) were calculated.

Moreover, the percent of the DT range (variance) relative to the observation range (variance) is also calculated to compare the spread in DT data and in observations. The range is estimated as the difference between the maximum and minimum values (outliers outside the range of mean ± two standard deviations are neglected). The range and variance together measure the spread of the data.

As stated earlier, the DT dataset was corrected for the SLP effect, so the tide-gauge observations need to be corrected before evaluating them against the DT data. Gaspar and Ponte (1997) subtracted the inverse barometer (IB) effect due to air pressure from the observed sea level using the following relationship:

$$\mathrm{IB}\ [\mathrm{m}] = \frac{-100 \times (\mathrm{SLP} - \mathrm{SLP_{ref}})}{\rho g}, \quad (1)$$

where $\mathrm{SLP_{ref}}$ [mbar] is the mean sea level pressure (SLP) over the ocean, ρ (=1027 kg m^{-3}) is the water density, and g (=9.8 m s^{-2}) is the gravity acceleration.

2.2.2. Altimetry dynamic topography (DT) data

The spatial and temporal distributions of southern Levantine sea-level variation are studied using the DT dataset over a 21-year period, focusing on seasonal and inter-annual distributions of average values and linear trends. Linear trends are calculated using ordinary least squares estimation and tested for significance using t-tests at a 95% significance level.

The effect of the NAOI on sea-level data needs to be corrected (Tsimplis et al., 2013) using a barotropic sea-level model forced by atmospheric pressure and wind. However, monthly DT is significantly correlated with the NAOI over only 38% of the southern Levantine sub-basin (data not shown). The effects of NAOI on MSL will, therefore, not be discussed here and are regarded as less important in the studied region than are other oceanic/weather components.

Seasonal and annual correlation coefficients (R) between DT and the other studied atmospheric/oceanic parameters (i.e., barotropic response through the Gibraltar Strait, SST, sea level west of the Gibraltar Strait, steric sea level, and ocean mass changes) are calculated to investigate their relationships with sea-level changes. The SST, sea level west of the Gibraltar Strait, and ocean mass datasets are freely downloadable from the Internet (Section 2.1).

Barotropic responses through the Gibraltar Strait due to sea-level changes were calculated based on the regression

model of Menemenlis et al. (2007) and Tsimplis et al. (2013), as follows:

$$h(t) = 0.5\tau_x(t) + 0.95\tau_y(t), \quad (2)$$

where h is the sea-level difference between the western and eastern sides of the Gibraltar Strait, τ_x and τ_y the zonal and meridional wind stress components, respectively, and t time in days.

The steric sea-level variations (Δz) related to changes in water density can be calculated from the effects of thermal expansion and saline contraction and are evaluated using the equation from Shaltout and Omstedt (2014), as follows:

$$\Delta z \cong -z[-\alpha\Delta T + \beta\Delta S], \quad (3)$$

where z is the water depth, α the thermal expansion coefficient at constant pressure and salinity, β the salt contraction coefficient at constant pressure and temperature, and ΔT and ΔS the changes in temperature and salinity, respectively.

2.2.3. GFDL model results over the study area

The results of the three GFDL realizations for the 1993–2013 period were first examined using the DT data. Next, the realization that best simulated the current sea-level changes was used in scenario studies.

The GFDL ZOS calculations were corrected for the SLP effect using Eq. (1). Monthly and annual averages of ZOS and DT were then calculated for a 21-year control period, 1993–2013. Biases in the linear trends were used to test the quality of each GFDL simulation and calculated as follows:

$$\text{Linear trend biase} = 100 \times \frac{\text{GFDL ZOS linear trend} - \text{Altimetry DT linear trend}}{\text{Altimetry DT linear trend}}\%. \quad (4)$$

Only GFDL simulations that simulated current sea levels reasonably well were used to illustrate the uncertainty of the projected sea level based on the CMIP5 scenarios.

Finally, the projected sea-level changes were compared with SRTM digital elevation data to study the flooding probability in the study area and to determine whether or not the Nile Delta coast will be threatened by the projected SLR during the twenty-first century.

3. Results

3.1. Observed sea level and DT altimetry datasets

In this section, the feasibility of using DT altimetry datasets in describing the sea level dynamics over the study area is investigated by determining the direct correlation between observed sea levels and altimetry data at five selected stations (Table 1).

The daily satellite DT data follow the daily observations well at a 95% significance level for all studied stations (Table 1). Moreover, the monthly DT values follow well with the monthly observations at a 95% significance level for coastal stations and at 90% significance level for open sea stations (i.e., shallow and deep-water stations). The satisfactory correlation between DT and coastal station results supports the previous finding of Rio et al. (2014) and indicates that the coastal DT usefully represents coastal sea level. The lower correlation for open sea stations (S04 and L04) incomparable with higher correlation at coastal stations runs counter to the fact that altimetry is less accurate along the coast, indicating that the S04 and S02 regions may have been influenced by a physical process such as strong currents during the studied period.

The DT data capture approximately 41–90% of the observed daily variance and approximately 61–161% of the observed monthly variance. Similarly, the DT data capture approximately 36–68% of the observed daily range and approximately 59–116% of the observed monthly range. Moreover, at Alexandria Harbour station (n = 13 years of observations), the DT data were significantly correlated with observations at a 95% significance level (R = 0.87). Annual DT range (variance) captured 86% (96%) of the observed values. The differences between the observations and the satellite altimeter data (DT) are acceptable, as the observations were collected every 10 s while the satellite altimeter data were measured every day. We conclude that the satellite altimetry

Table 1 Coefficients of correlation between observed sea level and DT satellite altimetry sea level at the five studied stations: n = number of observations, R = correlation coefficient; the percent of the DT range (variance) relative to the observation range (variance) is also given. Bold values indicate that the correlation is significant at a 95% significance level.

Station		Time span	N	R	Variance [%]	Range [%]
L01 (shallow water)	Daily	1 February 1999–31 January 2000	365	**0.40**	41	48
	Monthly		12	0.43	83	88
S04 (deep water)	Daily	1 May 1999–30 April 2000	366	**0.40**	42	36
	Monthly		12	0.41	61	59
Alexandria Harbour (along the shore)	Daily	1992–2006	5448	**0.74**	54	52
	Monthly		179	**0.87**	76	59
Alexandria (along the shore)	Daily	2010–2013	1461	**0.83**	64	68
	Monthly		48	**0.89**	89	100
Marsa Matrouh (along the shore)	Daily	2004	366	**0.47**	90	50
	Monthly		12	**0.55**	166	116

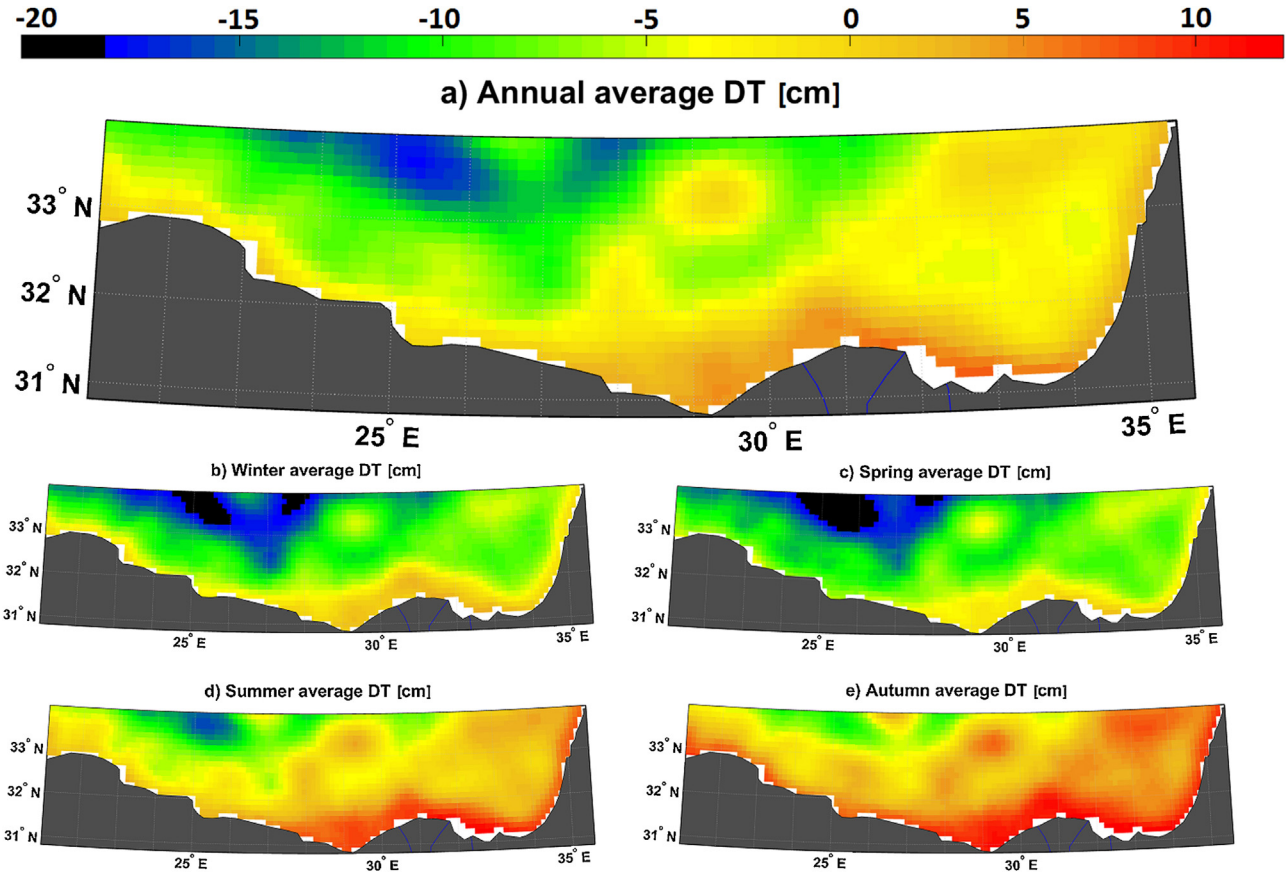

Figure 2 Spatial distribution of southern Levantine dynamic topography [cm] calculated from a 21-year period (1993–2013): (a) annual average, (b) winter, (c) spring, (d) summer, and (e) autumn.

data can be used in sea-level studies along the Egyptian coast and in studying long-term ocean dynamics on monthly or longer time scales.

3.2. Satellite altimetry DT data

3.2.1. Spatial and temporal DT distributions

The annual DT based on satellite data over the southern Levantine sub-basin ranged from +7.7 cm to −17.2 cm (Fig. 2), the maximum values occurring along the eastern Egyptian Mediterranean coast and the minimum values over the north-western part. This illustrates an annual SLR extending from open water towards the Egyptian coastal areas and associated partly with the coastal surface current characterizing this area (Shaltout and Omstedt, 2014).

Seasonal analysis of DT (Fig. 2) identifies the typical patterns of sub-regions where gyres are generated (e.g., the Marsa Matrouh gyre). The current analysis indicates that Marsa Matrouh gyres are anticyclonic in all seasons, in good agreement with previous findings of Menna et al. (2012), Poulain et al. (2012), and Amitai et al. (2010).

The seasonal and annual spatial patterns of the southern Levantine DT distribution are similar, but with marked seasonal variability. The maximum (minimum) values of average seasonal DT are 3.8 (−20.4), 1.7 (−21.8), 12.6 (−16), and 13.2 (−11) cm in winter, spring, summer, and autumn, respectively.

The annual DT trend in the studied region (Fig. 3) ranged from −1.8 cm decade^{-1} to +5.9 cm decade^{-1} (at the centre of the Marsa Matrouh gyre). Only approximately 0.5% (8.5%) of the study area displayed a negative (insignificant) DT trend, indicating that SLR dominated the studied period. Approximately 4.8% of the study area displayed trends exceeding 5 cm decade^{-1} and there was a seasonal DT trend distribution with maximum DT trends in winter and minimum in autumn.

Along the Egyptian Mediterranean coast, the annual DT trend increase was 3–5 cm decade^{-1} and 90% of this coast displayed annual DT trends of 3–4 cm decade^{-1}. The greatest DT trend along this coast occurred between Alexandria and Marsa Matrouh, with average values ranging between 5.5 cm decade^{-1} in winter and 3 cm decade^{-1} in autumn.

3.2.2. Statistical relationship between southern Levantine dynamic topography and various atmospheric/oceanic processes

In most of the southern Levantine sub-basin, sea levels are significantly correlated with the AAM sea levels, steric sea levels, and SST. However, sea-level changes related to winds (i.e., the barotropic response) through the Gibraltar Strait and changes in the ocean mass displayed non-significant correlations with sea levels in the southern Levantine sub-basin (Fig. 4).

Throughout the southern Levantine sub-basin, monthly sea level is directly correlated with AAM sea levels, especially

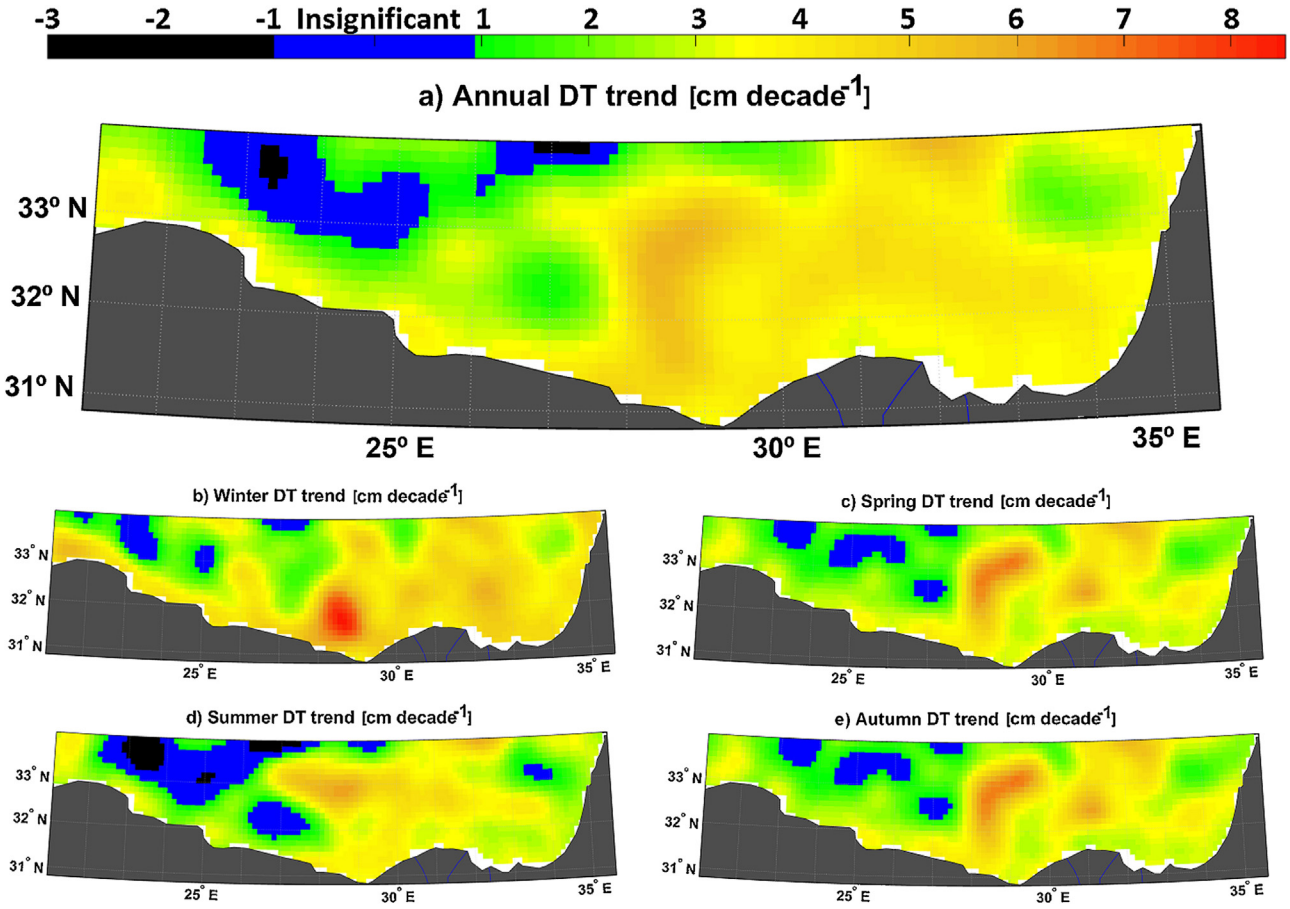

Figure 3 Linear trend distribution of southern Levantine dynamic topography [cm decade^{-1}] calculated for a 21-year period (1993–2013): (a) annual average, (b) winter, (c) spring, (d) summer, and (e) autumn.

over the eastern part and in winter (Fig. 4 and Table 2). This high monthly correlation suggests that the barotropic exchange through the Gibraltar Strait was the dominant factor affecting sea-level change in the study area. In addition, this high monthly correlation indicates that the atmospheric forced sea-level change may work in similar ways over both the AAM and southern Levantine sub-basins.

There is a significant direct relationship between monthly sea levels and steric sea levels over 99% of the southern Levantine sub-basin, especially in summer. This result supports previous findings discussed by Tsimplis and Rixen (2002), Quinn and Ponte (2010), and Shaltout and Omstedt (2014).

In general, there is a strong direct correlation between the monthly sea levels and SST over 97% of the southern Levantine sub-basin, most markedly in winter. This result is in good agreement with earlier findings discussed by Cazenave et al. (2001) and Shaltout and Omstedt (2014).

In contrast, there is a significant correlation between monthly sea level and barotropic response through the Gibraltar Strait (ocean mass) over only 24% (6%) of the southern Levantine sub-basin, most markedly in winter. This result stands in contrast to those of Tsimplis et al. (2013) and Landerer and Volkov (2013), illustrating how local and large-scale MSL features can differ significantly, especially sea-level response to barotropic response through the Gibraltar Strait and changes in ocean mass.

The effects of the studied oceanic/weather components on the daily and monthly sea level over the southern Levantine sub-basin display similar patterns (data not shown). The effects of the studied oceanic/weather components and sea levels on the seasonal time scale are presented in Table 2.

Annual correlations between sea level and the studied oceanic/atmospheric components (i.e., AAM sea level, steric sea level, SST, barotropic response through the Gibraltar Strait, and ocean mass) were significant over 83%, 49%, 73%, 24%, and 6% of the study area, respectively (Table 2). This indicates that the inter-annual correlations of AAM sea levels, steric sea levels, and SST (barotropic response through the Gibraltar Strait and ocean mass) explain less (more) of the southern Levantine sub-basin sea-level variability over the study area than do the monthly correlations.

The sensitivity of the correlations between the five studied components and sea level relative to time period using several sub-periods of DT data (i.e., 1993–2003, 1999–2009, and 2003–2013) indicates that all studied processes depend on time period and season, especially in winter (Table 2). These results indicate that steric effects were the dominant factor affecting sea levels in the 1999–2009 period, while AAM was the dominant factor affecting sea level during the 1993–2003 and 2003–2013 periods.

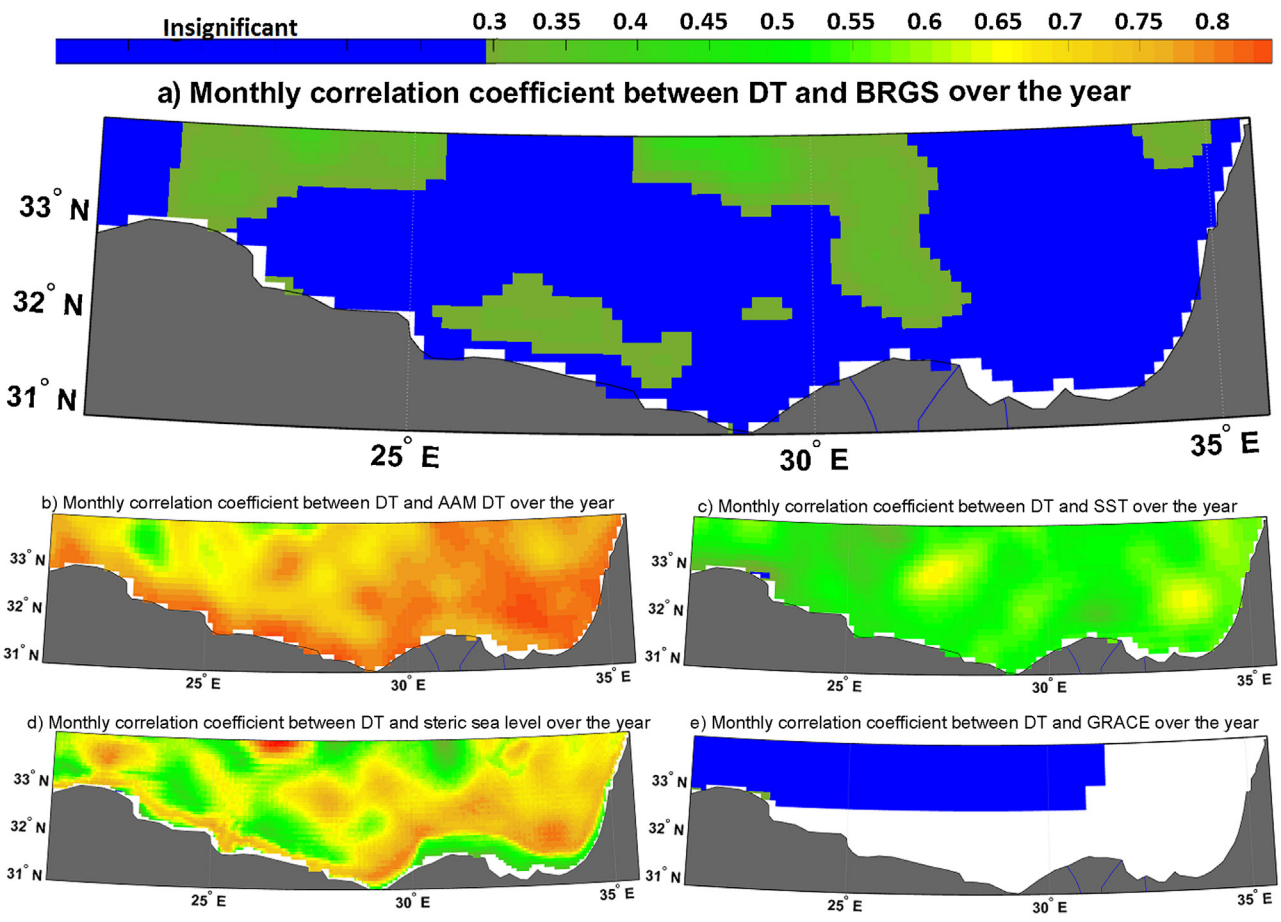

Figure 4 Monthly correlation coefficients between southern Levantine dynamic topography and the studied atmospheric/oceanic components; AAM = Active Atlantic Mediterranean sub-basin, BRGS = wind setup (i.e., barotropic response) through the Gibraltar Strait; white indicates missing data.

3.3. GFDL ZOS sea-level dataset

In this section, sea-level projections for the study area in the twenty-first century are studied using the results of three realizations of the GFDL model, i.e., GFDL-CM3, GFDL-ESM2G, and GFDL-ESM2M. The projected sea levels are based on four CMIP5 scenarios, i.e., RCP26, RCP45, RCP60, and RCP85, for the three model realizations.

3.3.1. Present conditions based on the control period, 1993—2013

The performance of the various GFDL simulations with the used RCP emission scenarios based on the calculated annual percentage of linear trend bias is shown in Fig. 5. The GFDL-CM3 simulation overestimates the altimetry sea-level trends by only approximately 0.3%. However, the other simulations underestimate the altimetry sea-level trends by approximately 1.3% and 0.6% for the GFDL-ESM2G and GFDL-ESM2M simulations, respectively. The simulations that best describe, relative to DT altimetry data, recent sea-level trends in the study area are GFDL-CM3 and GFDL-ESM2M, especially offshore from the Nile Delta region.

Two-model ensemble means (GFDL-2ENM) based on the two best GCM runs (i.e., GFDL-CM3 and GFDL-ESM2M) are calculated and presented in Fig. 5. This two-model ensemble scenario calculation underestimates the sea level trend by approximately 0.16%, which means that the GFDL-2ENM scenario underestimates the sea levels at the end of the examined period by only 0.015 cm, which is not significantly different (according to *t*-tests, 95% significance level) from observed altimetry data, particularly in the coastal area. We therefore use the GFDL-2ENM scenario when projecting sea-level changes to the end of the present century.

3.3.2. Future sea-level changes, 2006—2100

Thirty-year running annual means of projected GFDL-2ENM calculations indicate a significant SLR over the current century in the southern Levantine sub-basin. Average SLRs over the 2071—2100 period relative to the 2006—2035 period are expected to be 8.0, 9.5, 8.8, and 16.7 cm for the GFDL-2ENM model simulation using RCP26, RCP45, RCP60, and RCP85 emission scenarios, respectively (Fig. 6), less (more) increase occurring along the Egyptian Mediterranean coast (deep-water area) and in summer (winter) (Fig. 7).

In general, there is strong seasonal variability in sea levels (Fig. 7). In the study area, sea levels are expected to increase under all emission scenarios, most markedly in winter and under the RCP85 scenario and least markedly in summer and

Table 2 Monthly coefficients of correlation between sea level and the studied oceanic/atmospheric components over the study area ($n = 252$, 95% significance level); the percentage of the study area significantly correlated with the studied atmospheric components is shown.

	Study period	Annual [%]	Winter [%]	Spring [%]	Summer [%]	Autumn [%]
AAM sea levels	1993–2013	83	98	90	90	80
	1993–2003	70	98	71	94	54
	1999–2009	25	32	52	83	70
	2003–2013	84	91	88	86	90
Steric sea levels	1993–2013	49	78	77	87	78
	1993–2003	–	–	–	–	–
	1999–2009	81	93	96	91	87
	2003–2013	65	81	84	92	79
SST	1993–2013	73	100	78	67	48
	1993–2003	58	100	68	66	37
	1999–2009	23	89	57	41	63
	2003–2013	67	90	83	44	57
Barotropic response through the Gibraltar Strait	1993–2013	24	96	5	0	62
	1993–2003	70	98	71	94	54
	1999–2009	25	32	52	83	70
	2003–2013	84	91	88	86	90
Ocean mass	1993–2013	6	44	7	6	24
	1993–2003	–	–	–	–	–
	1999–2009	–	–	–	–	–
	2003–2013	6	44	7	6	24

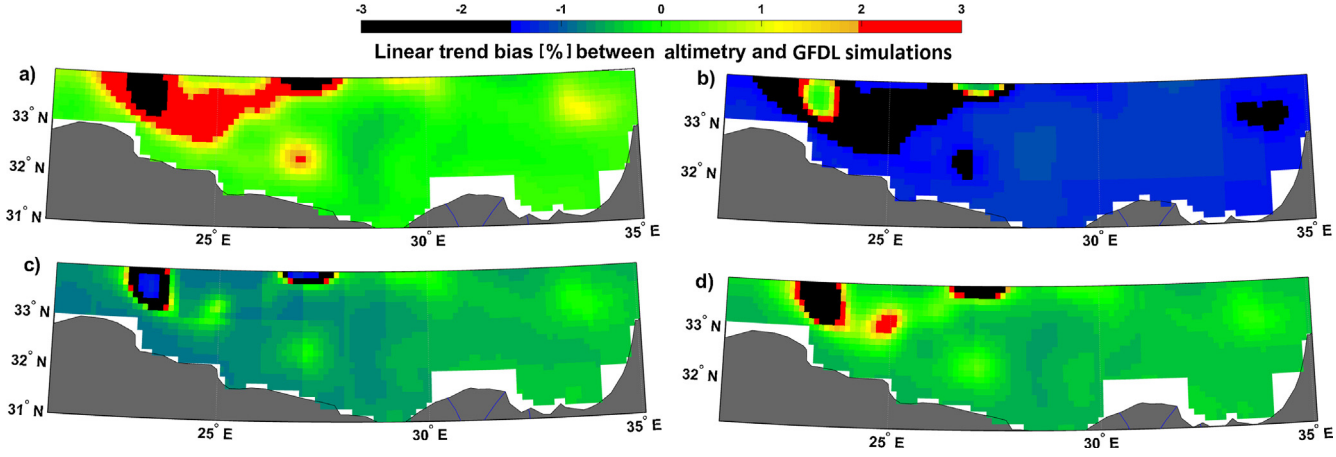

Figure 5 Performance of various studied GFDL simulations of the southern Levantine sub-basin in the control period (1993–2013) for the (a) GFDL-CM3, (b) GFDL-ESM2G, (c) GFDL-ESM2M, and (d) GFDL-2ENM simulations; white indicates missing data.

under the RCP60 scenario. Current results indicate a smaller SLR along the Egyptian Mediterranean coast than the average global SLR calculated using the same future scenarios (Kopp et al., 2014). In addition, the present calculated SLR along the Egyptian Mediterranean coast is less than that calculated by Tsimplis et al. (2008) for the whole Mediterranean Sea.

3.3.3. Uncertainty estimates

The present study takes account of three sources of uncertainty associated with the scenarios, seasonal variations, and regional variations; uncertainty associated with the realizations used was considered only for the two models considered the best at describing the study area sea level. Uncertainties in the sea level projected for the southern Levantine sub-basin at the end of the twenty-first century were estimated to be 5, 10, 2.8, and 5 cm depending on the realization used, scenario used, regional variations, and seasonal variations, respectively. The greatest estimated uncertainty thus originates from the emission scenario used.

Overall, the present estimates of the projected sea level are affected by a wide range of uncertainties, some related

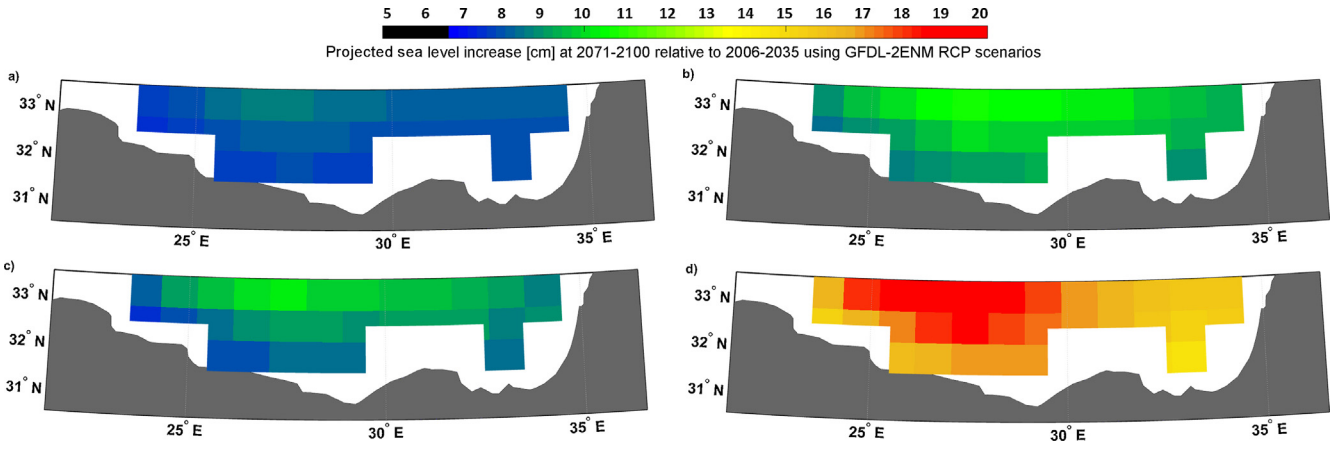

Figure 6 Projected sea level increase over the 2071—2100 period relative to the 2006—2035 period for the various GFDL-2ENM RCP scenarios, i.e., the (a) RCP 26, (b) RCP 45, (c) RCP 60, and (d) RCP 85 scenarios; white indicates missing data.

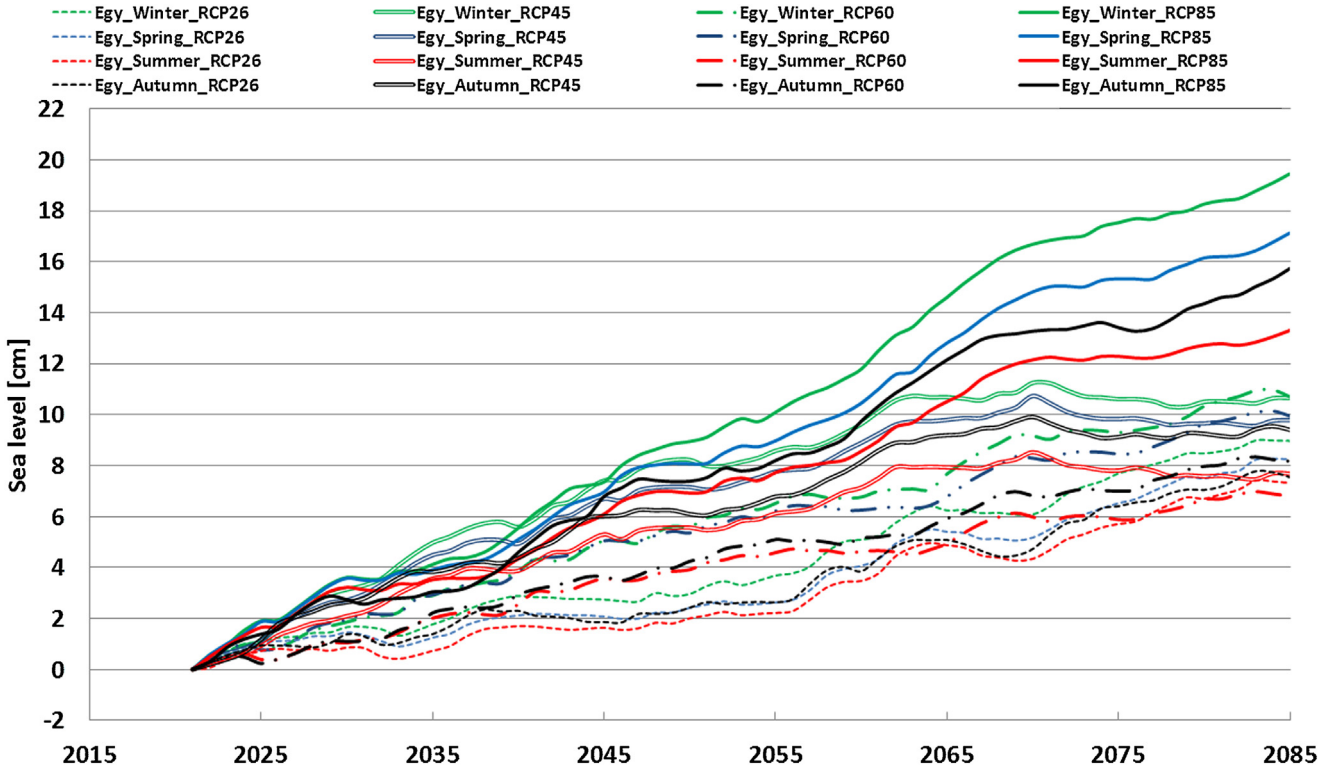

Figure 7 Thirty-year running annual mean sea levels for different seasons and emission scenarios relative to the 2006—2035 period for the GFDL-2ENM simulation.

to modelling and some related to management. These results call for various actions related to integrated coastal-zone management. This matter merits considerable attention and will be discussed in the following section.

3.3.4. Future flooding threats

Future risks of flooding can be studied by comparing digital elevation data maps and projected sea-level changes. Spatial analyses of digital elevation data in the study area (Fig. 8a) indicate that the area most sensitive to SLR is the Nile Delta coastal region (NDR). The land elevation of approximately 25% of the NDR is equal to or beneath present-day sea levels, mostly and particularly on the NDR's north-western side (Fig. 8b). Consequently, even a 10-cm SLR will dramatically damage the north side of the NDR, which includes large lakes, tourist resorts, historical sites, fertile agricultural land, and four populous cities: Alexandria, Rosetta, Borolus, and Port Said.

NDR subsidence on multi-century to millennial timescales has been dominated by the tectonic setting and earthquakes or by episodes of growth fault gravitational collapse rather than by sedimentation, whereas on shorter inter-seismic

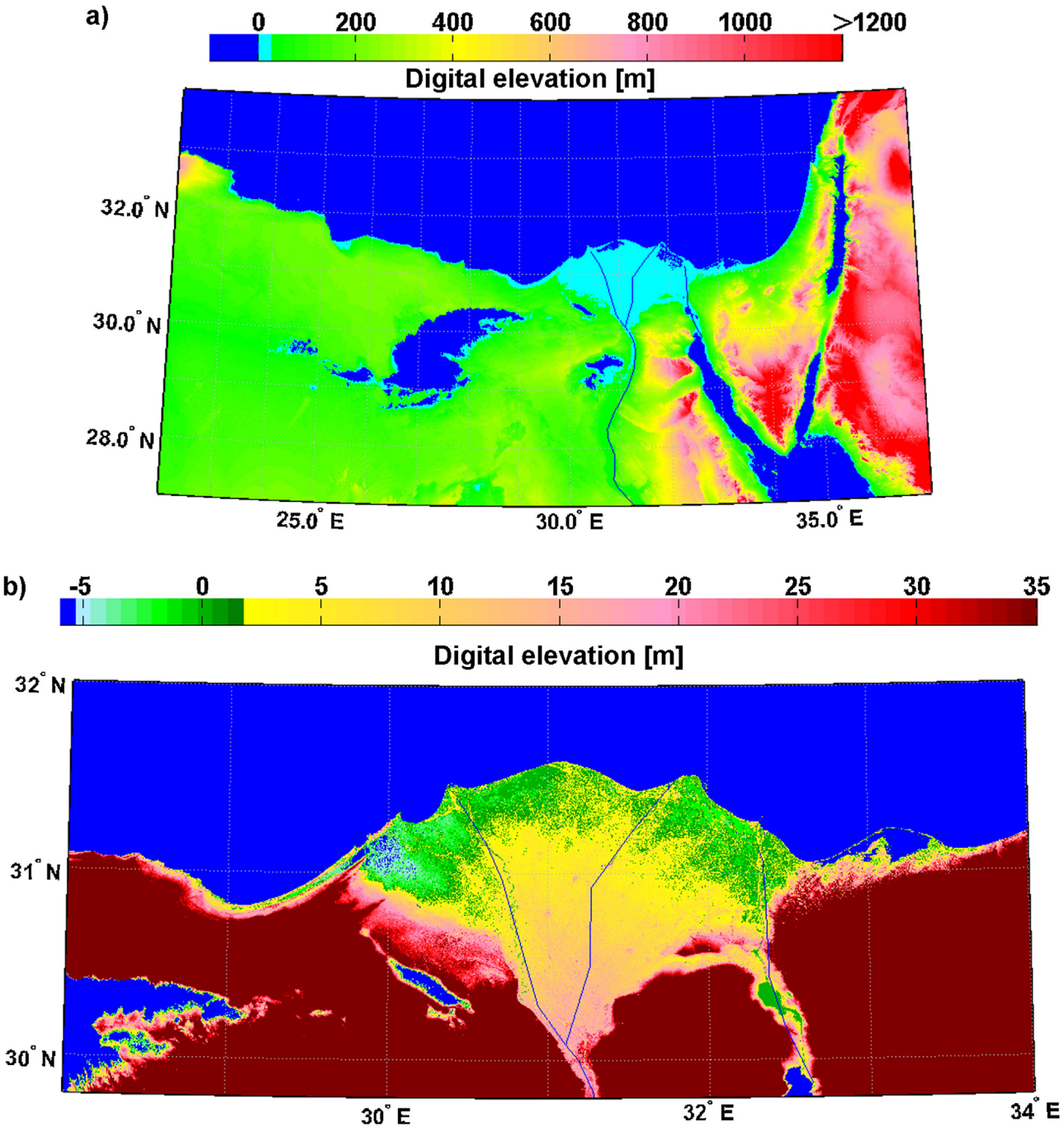

Figure 8 Digital elevation data for the southern Levantine sub-basin (a), zooming into the Nile Delta region (b).

decadal to century timescales, subsidence rates are likely steady and moderate (=0.4 cm decade^{-1}; Wöppelmann et al., 2013).

Over past millennial timescales: Alexandria, a highly populous and economically and historically important city on the NDR coast, has been subject to rapid subsidence attributable to the effects of the large tsunami generated by the AD 365 Crete earthquake and to subsequent seismic events (Guidoboni, 1994; Kebeasy, 1990). The greatest subsidence occurred from the seventh to tenth centuries CE, causing some of the structures built along Alexandria's Eastern Harbour to sink below the sea surface (McKenzie, 2007). A series of cross-sectional profiles reveal a ruined Ptolemaic/Roman pier over two thousand years old submerged by seawater in Alexandria's Eastern Harbour, its base (top) today lying −8 to −9 m (−5 to −6 m) below harbour waters (Goddio et al., 1998). Moreover, 180 heavy concrete blocks from Pharaonic/Ptolemaic times now lie about 30 m offshore from the eastern Alexandria Harbour (Fig. 9; Morcos et al., 2003).

The Lighthouse of Alexandria, regarded as one of the seven wonders of the ancient world, was completely destroyed by a series of earthquakes between the ninth and fourteenth centuries and remains underwater near the entrance to Alexandria's Eastern Harbour (Morcos et al.,

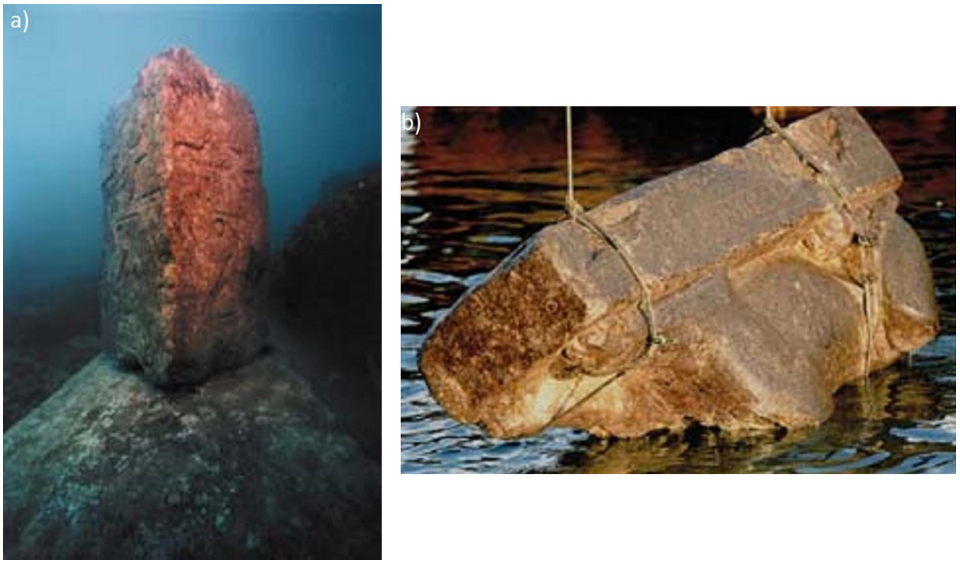

Figure 9 Two submerged archaeological objects: (a) an obelisk from the time of Sethi I at the moment of its discovery, and (b) raising a fragmentary sphinx with no inscriptions.
Photos: Stéphane Compoint/Sygma.

2003). At the end of the fifteenth century, Qait Bey Citadel was built on the site of the former lighthouse. Fig. 10 presents an interpretation of the appearance of the lighthouse reconstructed in the early twentieth century by Thiersch (1909).

Over the last century: Alexandrian sea-level data from 1944 to 2006, the longest available time series in the region, indicate two regimes (Fig. 11). Before the Aswan High Dam was built (1944—1963), Alexandrian sea levels display a strong significant rising trend of 0.5 cm year^{-1}; after the building of the dam (1964—2006), the Alexandrian sea-level trend is weaker at approximately 0.2 cm year^{-1}. The trend before 1963 is probably attributable to sedimentation from the Nile that caused sinking of the land surface. Since the building of the Aswan High Dam, less sediment has been exported and the rise is probably mainly attributable to climate change. These findings underlie our previous approach of neglecting vertical land motion associated with sediment transports and volcanic activity when studying sea levels over the coming century.

Figure 10 Three-tiered building of ancient Alexandria: the Pharos lighthouse (Thiersch, 1909).

Over the current century: The expected SLR along the NDR coast is calculated to range from +4 to +22 cm by 2100. Obviously, the NDR can remain safe from projected flooding during the current century only with effective integrated coastal-zone management.

4. Discussion

Comparing altimetry data with tide-gauge observations in the study area indicates that the satellite altimetry sea level data are representative of coastal sea-level observations. Consequently, altimetry data can be used in analysing the recent sea-level characteristics of the study area.

The observed recent sea-level trend in the southern Levantine sub-basin averages 3.1 cm decade^{-1}, close to the average Mediterranean sea level rise (SLR) calculated by Tsimplis et al. (2013) and Shaltout and Omstedt (2014).

Southern Levantine sub-basin sea levels are affected by several processes, including sea levels west of the Gibraltar Strait, steric sea levels, and sea-surface temperatures. The mean Mediterranean Sea responses to these three processes (Cazenave et al., 2001; Shaltout and Omstedt, 2014) are similar to the southern Levantine sub-basin responses. However the effects of changes in ocean mass and barotropic response through the Gibraltar Strait on the southern Levantine sub-basin sea level can be neglected, as the local and mean Mediterranean Sea responses to these two processes differ (Landerer and Volkov, 2013; Tsimplis et al., 2013). There is strong seasonal variation in the studied oceanic/weather processes, which also influences the sea-level characteristics in the study area. Moreover, the correlations between all the studied oceanic/weather processes and sea levels are dependent on the studied period.

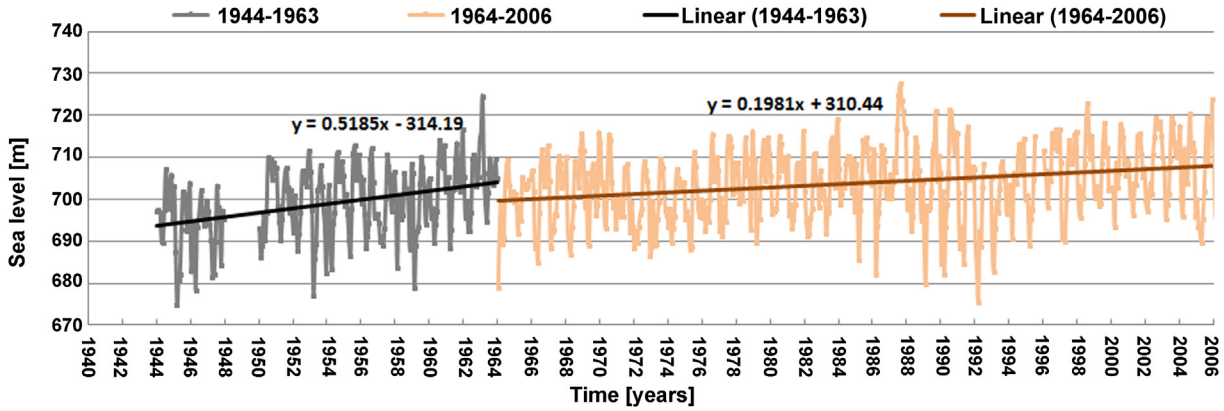

Figure 11 Significant linear trends at Alexandria Harbour station, 1944—2006.

This is the first study treating the dynamic projection of sea level along the Egyptian Mediterranean coast based on global climate modelling. Most earlier studies have only considered a range based on various assumptions (e.g., Hassaan and Abdrabo, 2013). In the present study, future southern Levantine sub-basin sea levels were described by calculating a Two-model ensemble means (GFDL-2ENM) based on GFDL-CM3 and GFDL-ESM2M, the GFDL-2ENM simulations that best describe recent sea-level trends offshore from the Nile Delta region. The variation in the SLR projected for the current century (i.e., 4—22 cm) was dominated by emissions, indicating that management efforts should emphasize emission reduction, though the building of protective barriers will also be needed. By 2100, we estimate that the southern Levantine sub-basin SLR will be less than estimated levels based on global average values (Kopp et al., 2014) or on earlier estimated mean sea levels for the Mediterranean Sea (Tsimplis et al., 2008). Highly accurate digital elevation data were used to study the land elevation above mean sea level to monitor the places most threatened by increased sea levels.

The Nile Delta region, which is less than 0.5 m above sea level, is clearly extremely vulnerable to SLR. Comparing projected twenty-first century SLR and digital elevation data indicates that the Nile delta region will not remain safe from flooding during the current century without effective adaptation measures, such as shore protection, emission reductions, and integrated coastal-zone management. This result agrees with the previous finding of Wöppelmann and Marcos (2012) but stands in contrast to that of Hanson et al. (2011). Wöppelmann and Marcos (2012) suggested that the Nile Delta region would be subject to moderate SLR, while Hanson et al. (2011) estimated an additional 0.5 m increase in Nile Delta sea level between 2005 and 2070.

Acknowledgements

This research was undertaken when Assoc. Prof. Mohamed Shaltout was a visiting scientist at the Ocean Climate Group, Department of Earth Sciences, University of Gothenburg, Sweden. The work is a contribution to GEWEX/BALTEX phase II, the new programme “Baltic Earth—Earth System Science for the Baltic Sea region”, and the HyMex programme. We would also like to thank Stephen Sanborn at Proper English for editing the text.

References

Abu Hatab, A., Xuexi, H., Shoumann, N., 2012. Exploring Egypt—China bilateral trade: dynamics and perspectives. J. Econ. Stud. 39, 314—326.

Amitai, I., Lehahn, Y., Lazar, A., Heifetz, E., 2010. Surface circulation of the eastern Mediterranean Levantine basin: insights from analyzing 14 years of satellite altimetry data. J. Geophys. Res. 115, C10058.

BACC II Author Team, 2015. Second Assessment of Climate Change for the Baltic Sea Basin. Springer International, Cham, Switzerland, 501 pp.

Cazenave, A., Cabanes, A., Dominh, A., Mangiarotti, S., 2001. Recent sea level changes in the Mediterranean Sea revealed by Topex/Poseidon satellite altimetry. Geophys. Res. Lett. 28, 1607—1610, http://dx.doi.org/10.1029/2000GL012628.

Chambers, D.P., Bonin, J.A., 2012. Evaluation of Release-05 GRACE time-variable gravity coefficients over the ocean. Ocean Sci. 8, 859—868.

Criado-Aldeanueva, F., Del Río, J., Vera, J., 2008. Steric and mass-induced Mediterranean sea level trends from 14 years of altimetry data. Glob. Planet. Change 60, 563—575, http://dx.doi.org/10.1016/j.gloplacha.2007.07.003.

Dasgupta, S., Laplante, B., Murray, S., Wheeler, D., 2009. Sea-Level Rise and Storm Surges. Policy Research Working Paper 4901. The World Bank, Development Research Group, Environment and Energy Team, Washington, DC.

Ducet, N., Le Traon, Y.P., Reverdin, G., 2000. Global high-resolution mapping of ocean circulation from TOPEX/Poseidon and ERS-1 and -2. J. Geophys. Res. 105, 19477—19498.

Dunne, P.J., John, G.J., Adcroft, J.A., Griffies, M.S., Hallberg, W.R., Shevliakova, E., Stouffer, J.R., Cooke, W., Dunne, A.K., Harrison, J.M., Krasting, P.J., Malyshev, L.S., Milly, P.C.D., Phillipps, J.P., Sentman, T.L., Samuels, L.B., Spelman, J.M., Winton, M., Wittenberg, T.A., Zadeh, N., 2012. GFDL's ESM2 global coupled climate—carbon earth system models. Part I: Physical formulation and baseline simulation characteristics. J. Clim. 25, 6646—6665, http://dx.doi.org/10.1175/JCLI-D-11-00560.1.

Dunne, P.J., John, J.G., Shevliakova, E., Stouffer, J.R., Krasting, P.J., Malyshev, L.S., Milly, P.C.D., Sentman, T.L., Adcroft, J.A., Cooke, W., Dunne, A.K., Griffies, M.S., Hallberg, W.R., Harrison, J.M., Levy, H., Wittenberg, T.A., Phillipps, J.P., Zadeh, N., 2013. GFDL's ESM2 global coupled climate—carbon earth system models. Part II: Carbon system formulation and baseline simulation

characteristics. J. Clim. 26, 2247–2267, http://dx.doi.org/10.1175/JCLI-D-12-00150.1.

Egyptian Environmental Affairs Agency (EEAA), 1999. The Arab Republic of Egypt: Initial National Communication on Climate Change. Prepared for the United Nations Framework Convention on Climate Change. Cairo.

El-Fishawi, N.M., Fanos, A.M., 1989. Prediction of sea level rise by 2100, Nile Delta coast. Int. Union Quat. Res. Quat. Shoreline Newslett. 11, 43–47.

El-Nahry, A.H., Doluschitz, R., 2010. Climate change and its impacts on the coastal zone of the Nile Delta. Environ. Earth Sci. 59, 1497–1506.

El-Raey, M., 1997. Vulnerability assessment of the coastal zone of the Nile delta of Egypt to the impacts of sea-level rise. Ocean Coast. Manage. 37, 29–40.

El-Raey, M., 2010. Impacts and implications of climate change for the coastal zones of Egypt. In: Michel, D., Pandya, A. (Eds.), Coastal Zones and Climate Change. Henry L. Stimson Center, Washington, DC, 31–50.

Frihy, O., 1992. Sea-level rise and shoreline retreat of the Nile Delta promontories, Egypt. Nat. Hazards 5, 65–81.

Frihy, O., 2003. The Nile Delta–Alexandria Coast: vulnerability to sea-level rise, consequences and adaptation. Mitig. Adapt. Strateg. Glob. Change 8, 115–138.

Gaspar, P., Ponte, R., 1997. Relation between sea level and barometric pressure determined from altimeter data and model simulations. J. Geophys. Res. 102, 961–971.

Goddio, F., Bernand, A., Bernand, E., Darwish, I., Kiss, Z., Yoyotte, J., 1998. Alexandria: The Submerged Royal Quarters. Periplus, London, 274 pp.

Gomis, D., Ruiz, S., Garcıa-Sotillo, M., lvarez Fanjul, E.A., Terradas, J., 2008. Low frequency sea level variability in the Mediterranean Sea. Part I: The contribution of atmospheric pressure and wind. Glob. Planet. Change 63, 215–229.

Griffies, S.M., Winton, M., Donner, L.J., Horowitz, W.L., Downes, S. M., Farneti, R., Gnanadesikan, A., Hurlin, J.W., Lee, H., Liang, Z., Palter, B.J., Samuels, L.B., Wittenberg, A.T., Wyman, B., Yin, J., Zadeh, N., 2011. The GFDL CM3 coupled climate model: characteristics of the ocean and sea ice simulations. J. Clim. 24, 3520–3544, http://dx.doi.org/10.1175/2011JCLI3964.1.

Guidoboni, E., 1994. Catalogue of Ancient Earthquakes in the Mediterranean Area up to the 10th Century. Istituto Nazionale di Geofisica, Bologna, 504 pp.

Hanson, S., Nicholls, R.J., Ranger, N., Hallegatte, S., Corfee-Morlot, J., Herweijer, C., Chateau, J., 2011. A global ranking of port cities with high exposure to climate extremes. Clim. Change 104, 89–111, http://dx.doi.org/10.1007/s10584-010-9977-4.

Hassaan, M.A., Abdrabo, M.A., 2013. Vulnerability of the Nile Delta coastal areas to inundation by sea level rise. Environ. Monit. Assess. 185, 6607–6616.

IPCC, 2013. In: Stocker, T.F., Qin, D., Plattner, G.-K., Tignor, M., Allen, S.K., Boschung, J., Nauels, A., Xia, Y., Bex, V., Midgley, P.M. (Eds.), Climate Change 2013: The Physical Science Basis. Contribution of Working Group I to the Fifth Assessment Report of the Intergovernmental Panel on Climate Change. Cambridge University Press, Cambridge, UK and New York, NY, USA, 1535 pp.

Kebeasy, R.M., 1990. Seismicity. In: Said, R. (Ed.), The Geology of Egypt. A.A. Balkema, Rotterdam, 51–59.

Kopp, R.E., Horton, R.M., Little, C.M., Mitrovica, J.X., Oppenheimer, M., Rasmussen, D.J., Strauss, B.H., Tebaldi, C., 2014. Probabilistic 21st and 22nd century sea-level projections at a global network of tide-gauge sites. Earth's Future 2, 383–406, http://dx.doi.org/10.1002/2014EF000239.

Landerer, F.W., Volkov, D.L., 2013. The anatomy of recent large sea level fluctuations in the Mediterranean Sea. Geophys. Res. Lett. 40, 553–557, http://dx.doi.org/10.1002/grl.50140.

McKenzie, J., 2007. The Architecture of Alexandria and Egypt, C. 300 B.C. to A.D. 700, vol. 63. Yale University Press, New Haven, CT, 458 pp.

Meehl, G.A., Stocker, T.F., Collins, W.D., Friedlingstein, P., Gaye, A. T., Gregory, J.M., Kitoh, A., Knutti, R., Murphy, J.M., Noda, A., Raper, S.C.B., Watterson, I.G., Weaver, A.J., Zhao, Z.C., 2007. Global climate projections. In: Solomon, S., Qin, D., Manning, M., Chen, Z., Marquis, M., Averyt, K.B., Tignor, M., Miller, H.L. (Eds.), Climate Change 2007: The Physical Science Basis. Contribution of Working Group I to the Fourth Assessment Report of the Intergovernmental Panel on Climate Change. Cambridge University Press, Cambridge, UK and New York, NY, USA.

Menemenlis, D., Fukumori, I., Lee, T., 2007. Atlantic to Mediterranean Sea level difference driven by winds near Gibraltar Strait. J. Phys. Oceanogr. 37, 359–376.

Menna, M., Poulain, P.-M., Zodiatis, G., Gertman, I., 2012. On the surface circulation of the Levantine sub-basin derived from Lagrangian drifters and satellite altimetry data. Deep-Sea Res. Part I 65, 46–58.

Milne, G.A., Gehrels, W.R., Hughes, C.W., Tamisiea, M.E., 2009. Identifying the causes of sea-level change. Nat. Geosci. 2, 471–478, http://dx.doi.org/10.1038/ngeo544.

Morcos, S., Tongring, N., Halim, Y., El-Abbadi, M., Awad, H., 2003. Towards Integrated Management of Alexandria's Coastal Heritage. Coastal Region and Small Island Papers 14. UNESCO, Paris, 79 pp.

Oddo, P., Adani, M., Pinardi, N., Fratianni, C., Tonani, M., Pettenuzzo, D., 2009. A nested Atlantic–Mediterranean Sea general circulation model for operational forecasting. Ocean Sci. 5, 461–473.

Palmer, A., 2008. Rising sea levels. The World Bank Report. Available at: http://www.theworldincrisis.com/artman2/publish/climate/Rising_Sea_Levels.shtml.

Poulain, P., Menna, M., Mauri, E., 2012. Surface geostrophic circulation of the Mediterranean Sea derived from drifter and satellite altimeter data. J. Phys. Oceanogr. 42, 973–990.

Quinn, J., Ponte, M., 2010. Uncertainty in ocean mass trends from GRACE. Geophys. J. Int. 181, 762–768, http://dx.doi.org/10.1111/j.1365-246X.2010.04508.x.

Rio, M.-H., Pascual, A., Poulain, P.-M., Menna, M., Barceló, B., Tintoré, J., 2014. Computation of a new mean dynamic topography for the Mediterranean Sea from model outputs, altimeter measurements and oceanographic in situ data. Ocean Sci. 10, 731–744.

Roaf, S., Crichton, D., Nicol, F., 2005. Adapting Buildings and Cities for Climate Change: A 21st Century Survival Guide. Elsevier, London, 400 pp.

Said, M.A., Moursy, Z.A., Radwan, A.A., 2012. Climate change and sea level oscillations off Alexandria, Egypt. In: Proceedings of the International Conference on Marine and Coastal Ecosystem, MarCoastEcs2012, Tirana, Albania, 25–28 April 2012, 353–359.

Shaltout, M., Omstedt, A., 2014. Recent dynamic topography changes in the Mediterranean Sea analyzed from altimetry data. CDO 7, 1–26.

Stammer, D., Cazenave, A., Ponte, R.M., Tamisiea, M.E., 2013. Causes for contemporary regional sea level changes. Annu. Rev. Mar. Sci. 5, 21–46, http://dx.doi.org/10.1146/annurev-marine-121211-172406.

Suzuki, T., Ishii, M., 2011. Regional distribution of sea level changes resulting from enhanced greenhouse warming in the Model for Interdisciplinary Research on Climate version 3.2. Geophys. Res. Lett. 38, L02601, http://dx.doi.org/10.1029/2010GL045693.

Taylor, K., Stouffer, R., Meehl, G., 2012. An overview of CMIP5 and the experiment design. BAMS 93, 485–498, http://dx.doi.org/10.1175/BAMS-D-11-00094.1.

Thiersch, H., 1909. Der Pharos, Antike Islam und Occident. Ein Beitrag zu Architekturgeschichte. B. G. Teubner, Leipzig and Berlin, 220 pp.

Tsimplis, M.N., Calafat, M.F., Marcos, M., Jordà, G., Gomis, D., Fenoglio-Marc, L., Struglia, V.M., Josey, A.S., Chambers, P.D., 2013. The effect of the NAO on sea level and on mass changes in the Mediterranean Sea. J. Geophys. Res. 118, 1–9, http://dx.doi.org/10.1002/jgrc.20078.

Tsimplis, M.N., Marcos, M., Somot, S., 2008. 21st century Mediterranean sea level rise: steric and atmospheric pressure contributions from a regional model. Glob. Planet. Change 63, 105–111.

Tsimplis, M.N., Rixen, N., 2002. Sea level in the Mediterranean Sea: the contribution of temperature and salinity changes. Geophys. Res. Lett. 29 51-1–51-4.

Volkov, D.L., Larnicol, G., Dorandeu, J., 2007. Improving the quality of satellite altimetry data over continental shelves. J. Geophys. Res. 112, C06020, http://dx.doi.org/10.1029/2006JC003765.

Wöppelmann, G., Le Cozannet, G., de Michele, M., Raucoules, D., Cazenave, A., Garcin, M., Hanson, S., Marcos, M., Santamaría-Gómez, A., 2013. Is land subsidence increasing the exposure to sea level rise in Alexandria, Egypt? Geophys. Res. Lett. 40, 2953–2957, http://dx.doi.org/10.1002/grl.50568.

Wöppelmann, G., Marcos, M., 2012. Coastal sea level rise in southern Europe and the nonclimate contribution of vertical land motion. J. Geophys. Res. 117, C01007, http://dx.doi.org/10.1029/2011JC007469.